Electronic Supplementary Information

A Universal Oxygen-Electrode for Reversible Solid Oxide Electrochemical Cells at Reduced Temperatures

Jun Hyuk Kim[a,†], Dongyeon Kim[b,†], Sejong Ahn[c,†], Kyeong Joon Kim[b], SungHyun Jeon[c], Dae-Kwang Lim[c,d], Jun Kyu Kim[c,e], Uisik Kim[c,d], Ha-Ni Im[b], Bonjae Koo[f], Kang Taek Lee[b,g,*], WooChul Jung[c,g,*]

[a] Department of Chemical Engineering, Hongik University, Seoul, Republic of Korea

[b] Department of Mechanical Engineering, KAIST, Daejeon, Republic of Korea

[c] Department of Materials Science and Engineering, KAIST, Daejeon, Republic of Korea

[d] Korea Electric Power Corp. Research Institute, Daejeon 34056, Republic of Korea

[e] Current address: Samsung Carbon Capture Research Institute, Samsung Advanced Institute of Technology (SAIT), Samsung Electronics Co., Ltd., Suwon 16678, Republic of Korea

[f] School of Chemistry and Energy, Sungshin Women's University, 2 Bomun-ro 34da-gil, Seoul, 02844, Republic of Korea

[g] KAIST Institute for the NanoCentury, Daejeon, Republic of Korea

[*] e-mail : leekt@kaist.ac.kr, wcjung@kaist.ac.kr

[†] These authors contributed equally.

Experimental Procedures

Material synthesis

$BaCo_{1-x}Ta_xO_{3-\delta}$ (x=0, 0.1, 0.2, 0.3, 0.4) powder is prepared through typical solid-state reaction method. Stoichiometric amounts of high purity Barium carbonate ($BaCO_3$, Alfa Aesar), Cobalt oxide (Co_3O_4, Sigma Aldrich), Tantalum oxide (Ta_2O_5, Sigma Aldrich) were ball-milled with zirconia ball using ethanol media for 24 hours. Then the solution is dried at 90^{o}C oven for 24 hours to completely evaporate ethanol. The obtained powders are pelletized into green body and subsequently calcined at 1200^{o}C for 10 hours. Resulting dense pellets were crushed with agar mortar, and another ball-milling with ethanol solvent is followed to make fine powders. Above steps (calcination and milling) are repeated twice to ensure phase formation.

Physical characterization

The crystal structures of the synthesized powders were analyzed by high-resolution X-ray diffraction (X'pert-PRO MRD). Cs-corrected scanning transmission electron microscope (JEOL) was used to characterize lattice plane of BCT20. Thermal expansion coefficients of BCO, BCT10, and BCT20 were analyzed between room temperature and 700^{o}C *via* High temperature X-ray diffractometer (D/MAX-2500, Rigaku) under ambient air. Heating rate of the samples were 5^{o}C min^{-1} with a 5 minutes hold before each scan. Scan speed was 4^o min^{-1} with a step size of 0.01^o. The microstructure of the half cells and single cells were characterized by SEM (Hitachi S-4800). O_2-TPD was measured using AutoChem II 2920 (Micromeritics). Samples were analyzed at 50~930^{o}C with heating rates as 10^{o}C min^{-1}. During the analysis He gas was supplied with a flow rate of 30 ml min^{-1}.

Fabrication and electrochemical measurements of symmetric cells

The interfacial polarization resistance or the area specific resistance (ASR) of the developed oxygen-electrode materials were evaluated using symmetric cells. Dense electrolyte pellets of SDC or BZCYYb were fabricated as followed: SDC powders (Fuelcellmaterials) or BZCYYb Powders (Kceracell) were first dry-pressed with a square steel die. Then the green body was sintered at 1450^{o}C for 5 hours to form dense electrolyte pellet. Thereafter, oxygen-electrode slurries were screen-printed on both sides of the electrolytes and fired at 900^{o}C for 2 hours in ambient air to complete symmetric cell fabrication. Oxygen-electrode slurries were made by mixing the respective oxygen-electrode powders with ink vehicle (Fuelcellmaterials) in a weight ratio of 1:1. Excess ethanol was initially added to aid facile ball-milling of the oxygen-electrode slurries for 24 hours, however later evaporated in 90^{o}C oven to finalize oxygen-electrode slurry preparation. Current collector of Ag paste is used for electrochemical measurements.

Biologics VSP-300 workstation is used for electrochemical measurements. For half-cell tests, fabricated symmetric cells were loaded on in-lab designed alumina chamber with a pseudo-four-configuration probe made from Pt-Ir wire. AC impedance measurements at OCV is conducted from 1 MHz to 0.01 Hz in the temperature range of 450~650^{o}C. Gas mixture of O_2 and Ar are flowed to make desired pO_2 in alumina tube. To introduce water vapor, temperature controlled bubbler was used. Water partial pressure (pH_2O) was monitored through a Dewpoint Meter (Model DM70).

In symmetric cell measurements, data points between two intercepts of the impedance arc on the real axis were extracted. The impedance arcs were scaled to the area of the electrode (0.2826 cm^2). The resistance value was halved as the original arc is a summation of both sides of the electrodes in symmetric cells. Resultingly, the half-cell electrode resistance is obtained.

Fabrication and electrochemical characterization of oxygen-conducting SOC

Single cell with fuel-electrode-supported configuration was devised to conduct fuel cell measurements. Two types of button cells were fabricated: SDC based single cell (Ni-SDC|SDC|BCT20) and GDC based analog (Ni-GDC10|GDC20|BCT20). To make SDC based single cell, NiO, SDC (Fuelcellmaterials), and starch were ball-milled in weight ratio of 6:4:1 to make fuel-electrode powders. Here the starch is fugitive pore former. The resulting powders were die-pressed and lightly fired at 950^{o}C for 1 hours. On top of the fuel-electrode pellets, electrolyte suspension slurry was drop-coated and subsequently sintered at 1400^{o}C for 5 hours to prepare fuel-electrode-electrolyte bilayered support. Electrolyte suspension slurry was made by mixing electrolyte powder with organic binder comprised with polyvinylpyrrolidone (PVP, Alfa Aesar), butyl benzyl phthalate (Alfa Aesar), triethanolamine (Alfa Aesar), and terpineol (Alfa Aesar). Oxygen-electrode slurry are screen-printed on electrolyte side and fired at 900^{o}C for 2 hours. GDC based single cell was prepared as followed: NiOGDC-P (part #. 131101) powder purchased from Fuelcellmaterials were dry pressed with square steel die. Electrolyte suspension slurry of GDC20 (Fuelcellmaterials) is then drop-coated on top of the resulting fuel-electrode pellets. Electrolyte suspension slurry was made similar to SDC electrolyte slurry. Then the fuel-electrode-electrolyte bilayer was sintered at 1500^{o}C for 5 hours. On the densified electrolyte, oxygen-electrode slurry was screen printed and fired at 900^{o}C for 2 hours. An ScSZ electrolyte-based single cell with a gelatin-derived SNDC thin interlayer was fabricated via tape casting, lamination, and co-sintering processes.[1] For three single cells, Ag paste was used as current collector.

Biologics VSP-300 workstation is used for electrochemical measurements. I-V characterization of the single cell was measured with 0.03 V s^{-1} scan rates. An in-lab-

constructed fuel cell testing station is utilized. Synthetic air (N_2: 79%, O_2: 21%) is blown to oxygen-electrode side with 100 sccm, while H_2 is blown to fuel-electrode side with 50 sccm.

Fabrication and electrochemical characterization of proton-conducting SOC

The fuel-electrode-supported proton-conducting SOC with a configuration of NiO-BZCYYb|BZCYYb|BCT20 was fabricated by a tape-casting and co-sintering process. The NiO-BZCYYb fuel-electrode supporting layer (FSL) slurry was prepared by mixing the NiO (Sumitomo) and BZCYYb (Kceracell) powder in a weight ratio of 6:4 with an organic solvent, binder and pore former. For fuel-electrode functional layer (FFL) slurry, the procedure was same as preparing FSL except that a pore former was excluded. Also, an electrolyte layer (EL) slurry was prepared by conducting a similar process without NiO powder. As-prepared each slurry was cast onto the PET film. The FSL, FFL and EL films were sequentially laminated and then pre-sintered at 900 ℃ for 3 h, followed by sintered at 1400 ℃ for 5 min in air using microwave furnace (UMF-04, Unicera, Korea).[2] After sintering, BCT20 oxygen-electrode was coated with an active area of 0.5 cm^2 onto the BZCYYb electrolyte by screen printing the BCT20 paste. BCT20 electrode was sintered at 850 ℃ for 3 min in air.

Pt meshes (Alfa Aesar) were attached at both electrodes of single cell, followed by mounted the single cell onto the alumina tube and sealed using the Ceramabond 571 (Aremeco). Humidified H_2 (3% H_2O) was supplied as fuel to the fuel electrode and air was applied to oxygen-electrode with each flow rate of 200 sccm during fuel cell test. For the electrolysis test, humidified H_2 (3% H_2O) and air (3% H_2O) were fed with same gas condition as in fuel

cell mode. The electrochemical performances were evaluated by a potentiostat (Bio-Logic, VMP-300) at operating temperature from 450 to 650 ℃. Impedance spectra was measured under open circuit voltage (OCV) in the frequency range from 1MHz to 0.1 Hz with an AC amplitude of 50 mV.

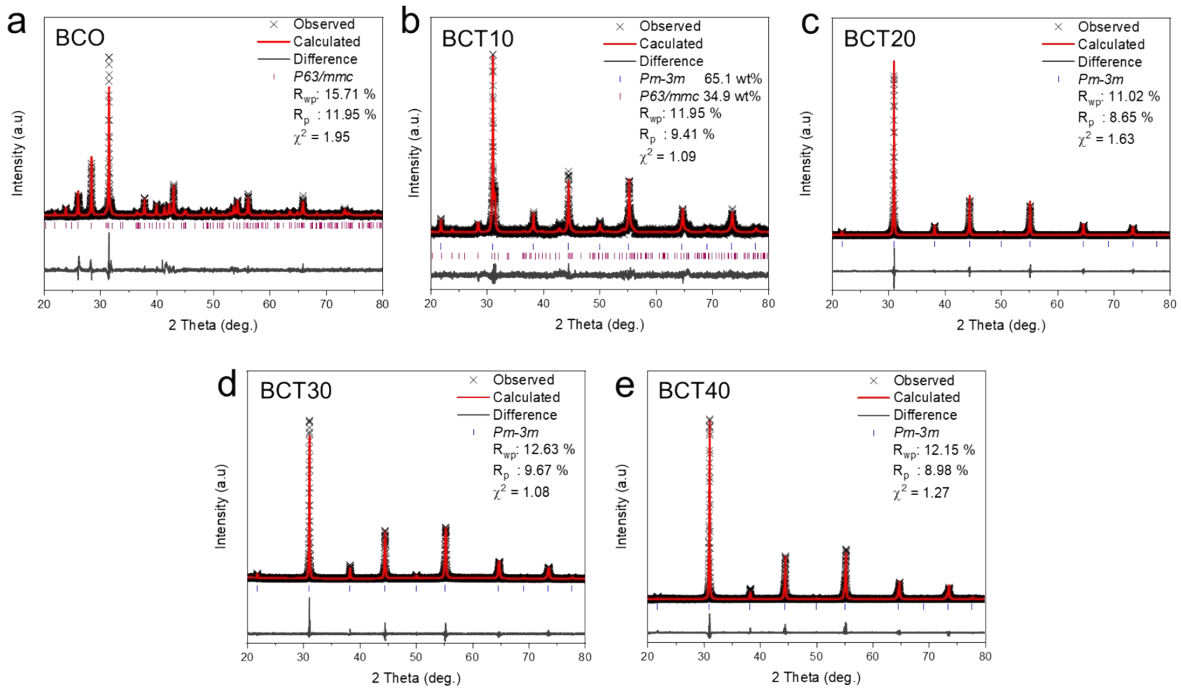

Figure S1. Rietveld refinement profiles of BCO, BCT10, BCT20, BCT30, and BCT40.

Table R1. Rietveld refinement results of BCO, BCT10, BCT20, BCT30, and BCT40.

Sample	Proportion (wt %)	Space group	a (Å)	b (Å)	c (Å)	R_p (%)	R_{wp} (%)	R_B (%)	χ^2
BCO	100	*P63/mmc*	5.663	5.663	28.508	11.95	15.71	7.80	1.95
BCT10	65.1 34.9	*Pm-3m* *P63/mmc*	4.071 5.691	4.071 5.691	4.071 28.477	11.95	9.41	3.98 6.25	1.09
BCT20	100	*Pm-3m*	4.085	4.085	4.085	8.65	11.02	3.82	1.63
BCT30	100	*Pm-3m*	4.076	4.076	4.076	9.67	12.63	3.35	1.08
BCT40	100	*Pm-3m*	4.071	4.071	4.071	8.98	12.15	3.63	1.27

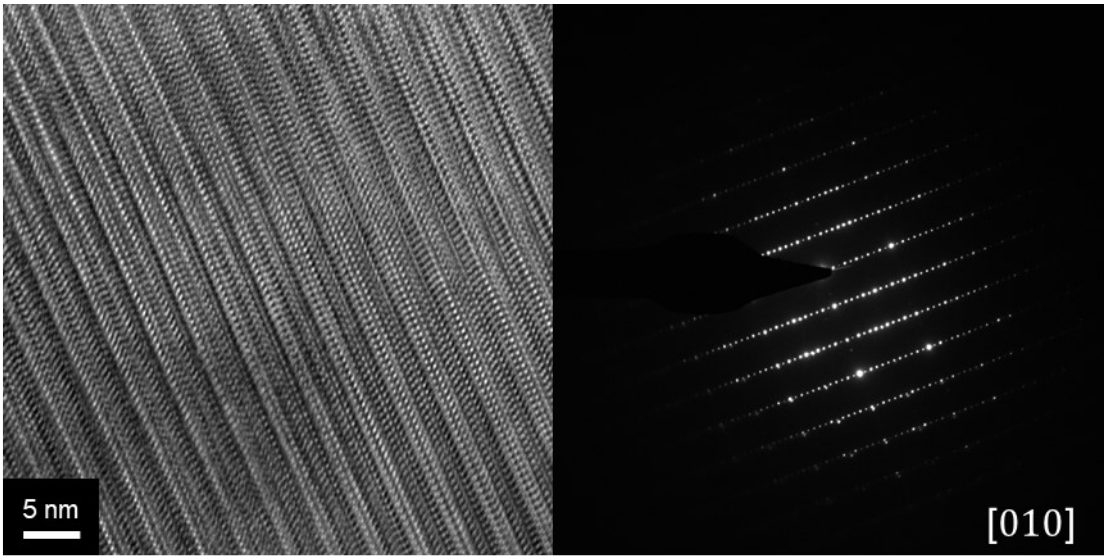

Figure S2. High-resolution transmission electron microscopy (HRTEM) image and SAED pattern of BCO (hexagonal).

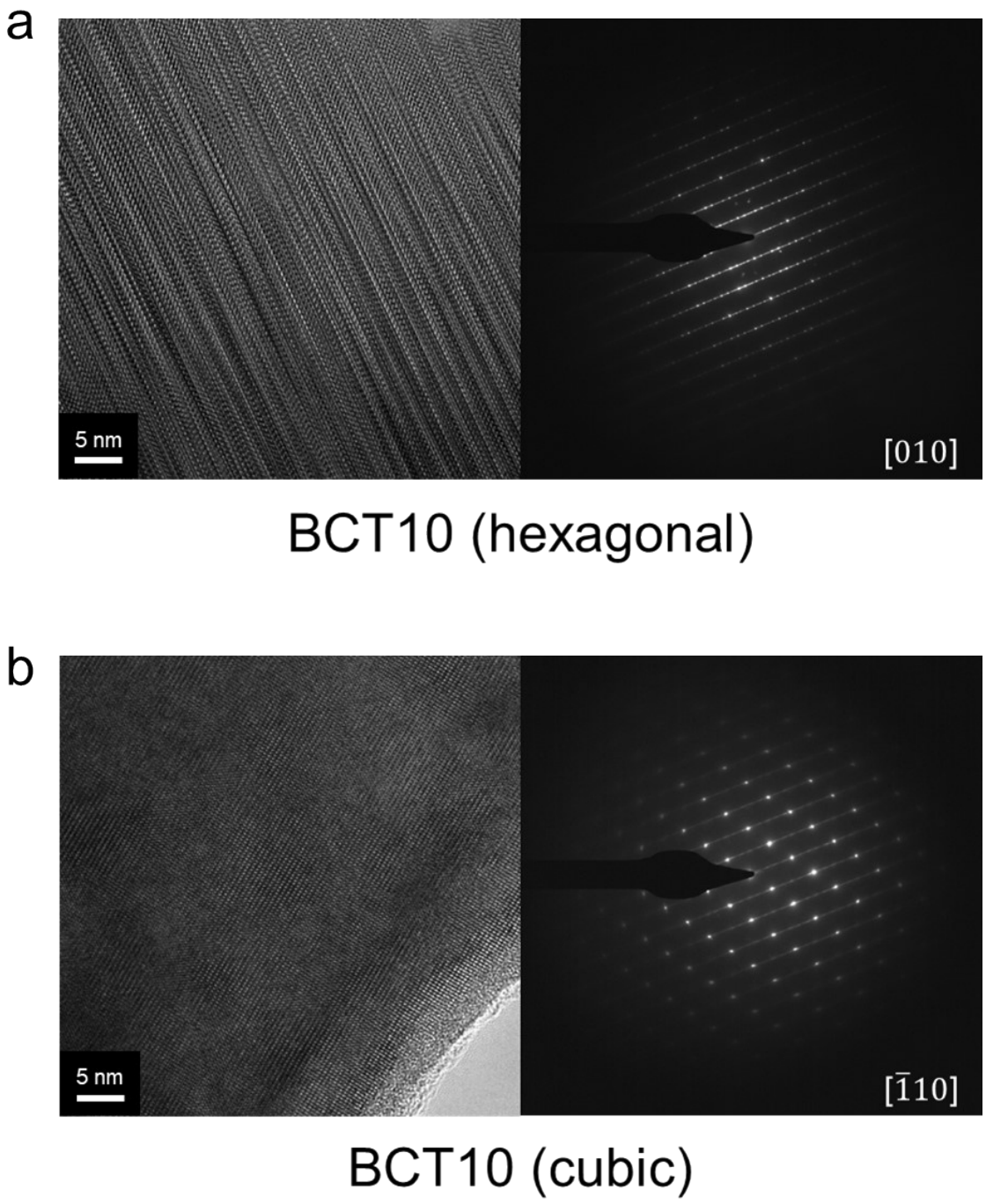

Figure S3. High-resolution transmission electron microscopy (HRTEM) image and SAED pattern of (a) BCT10 (hexagonal part), and (b) BCT10 (cubic part).

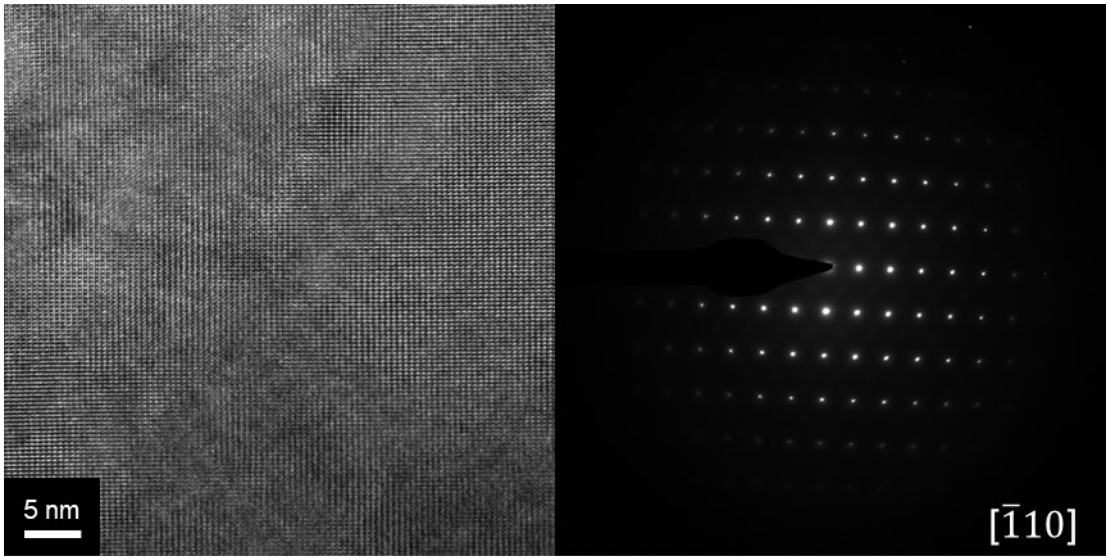

Figure S4. High-resolution transmission electron microscopy (HRTEM) image and SAED pattern of BCT20 (cubic).

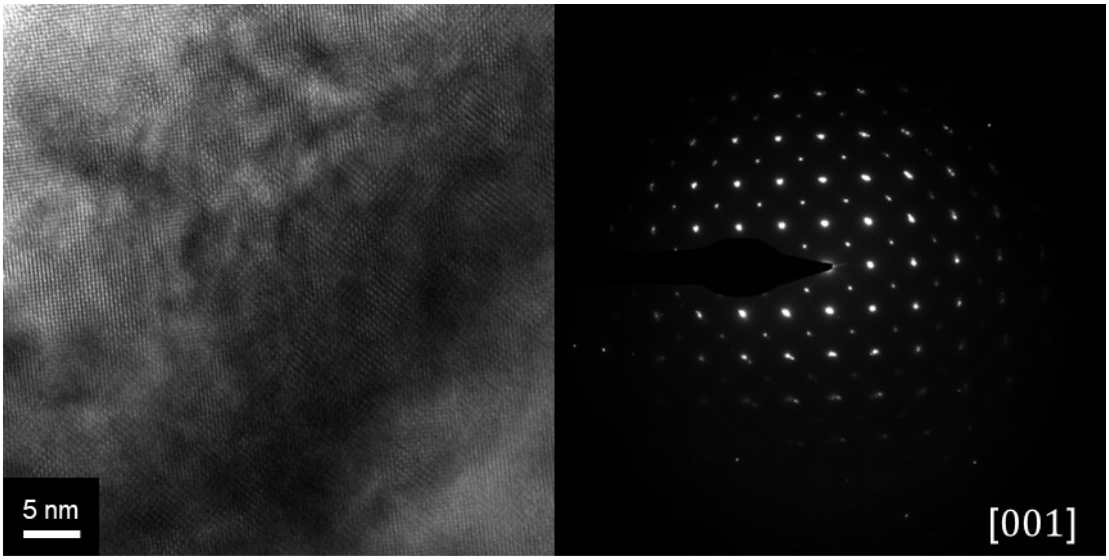

Figure S5. High-resolution transmission electron microscopy (HRTEM) image and SAED pattern of BCT30 (cubic).

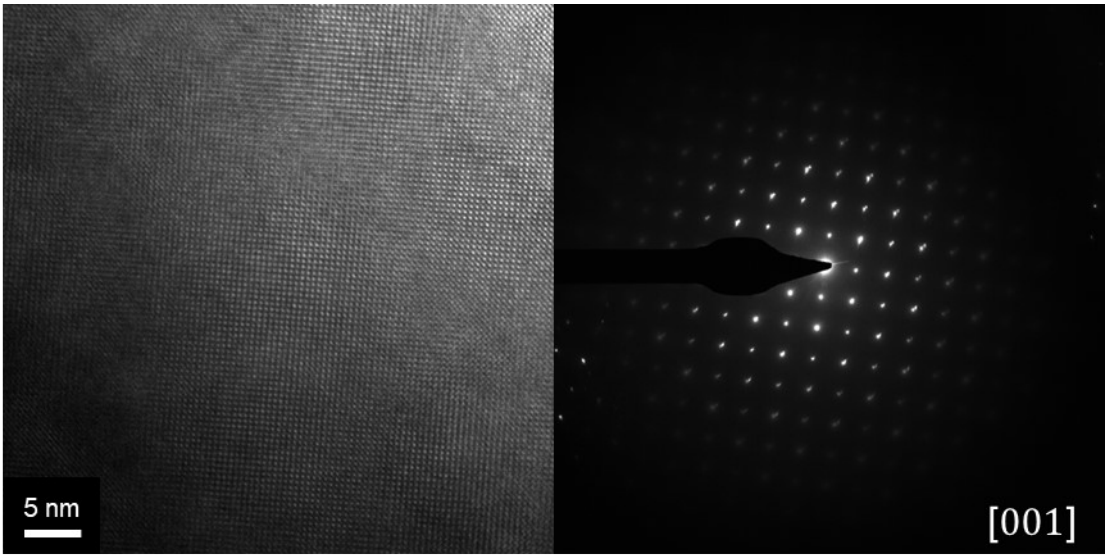

BCT40

Figure S6. High-resolution transmission electron microscopy (HRTEM) image and SAED pattern of BCT40 (cubic).

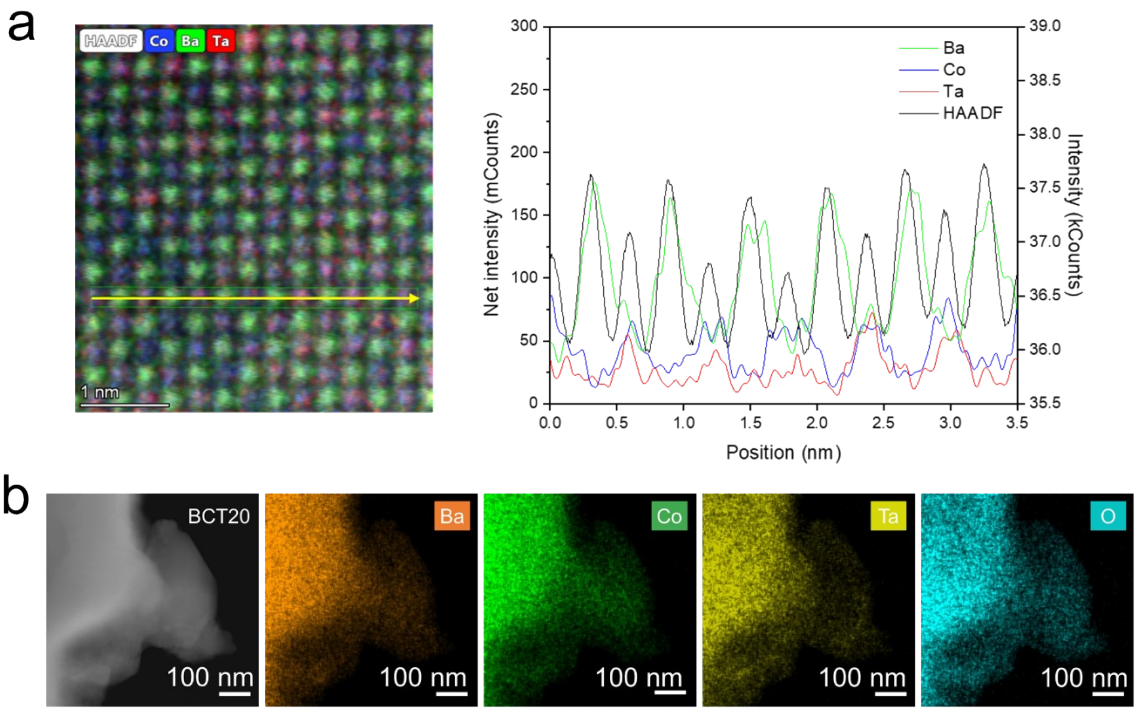

Figure S7. (a) Line-scan EELS for BCT20. (b) a high-angle annular dark-field scanning transmission electron microscopy (HAADF-STEM) and elemental mapping of BCT20 at lower magnification.

Supplementary note:

Ta is known to have blunt signal for EELS, so it is not frequently used to check atomic distribution. Thus the HADDF and EDS analysis shown in Figure 1d is the most suitable method to represent atomic distribution which is a typical result supporting homogenous distribution.[3]

Table S2. ICP-OES results of BCO, BCT10, BCT20, BCT30 and BCT40 samples.

Target Composition	Measurement by ICP-OES / at. %		
	Ba	Co	Ta
$BaCoO_{3-\delta}$	51.26	48.73	0
$BaCo_{0.9}Ta_{0.1}O_{3-\delta}$	50.14	44.96	4.90
$BaCo_{0.8}Ta_{0.2}O_{3-\delta}$	50.44	39.58	9.98
$BaCo_{0.7}Ta_{0.3}O_{3-\delta}$	50.82	34.45	14.73
$BaCo_{0.6}Ta_{0.4}O_{3-\delta}$	51.06	29.30	19.63

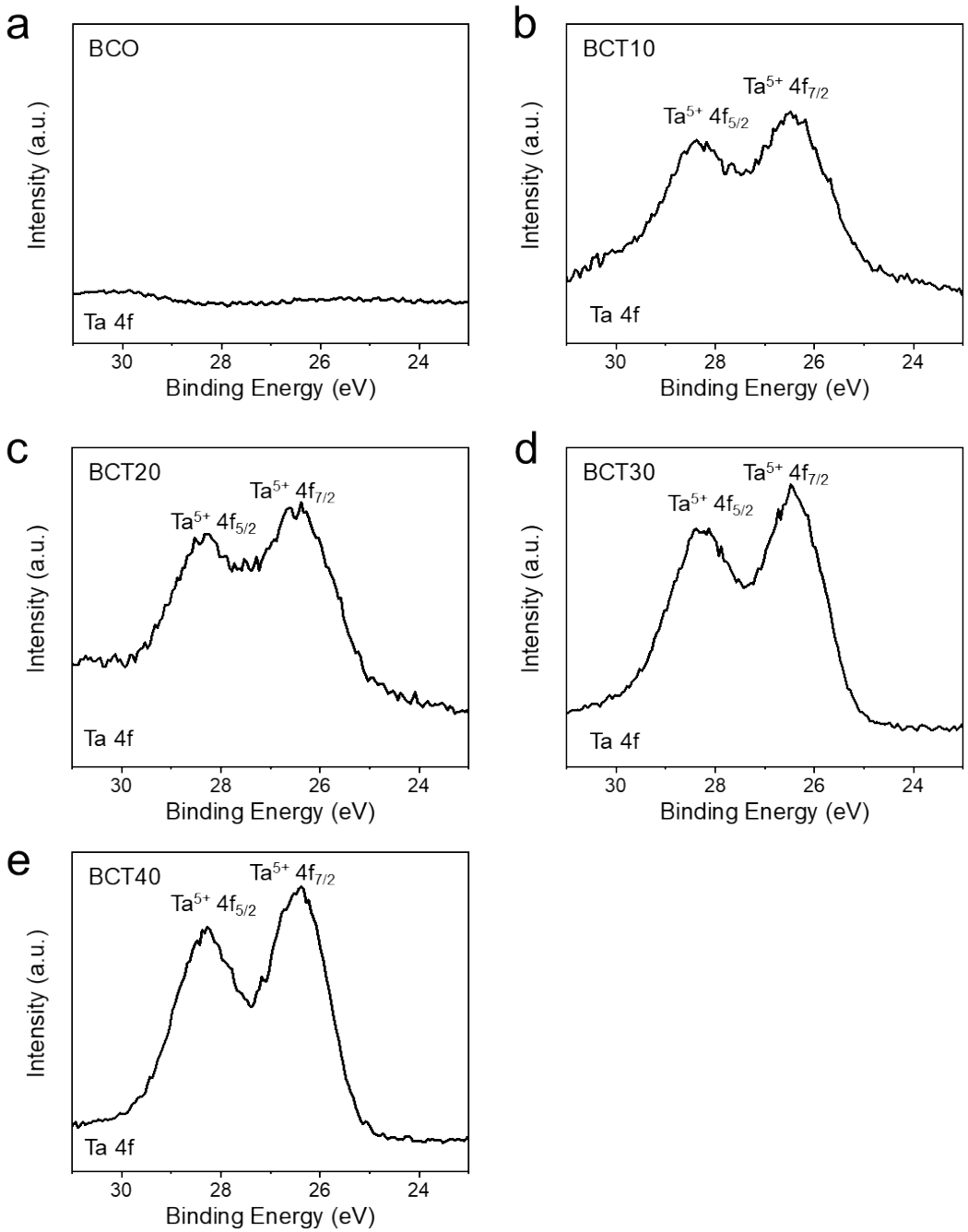

Figure S8. XPS spectra of Ta 4f for (a) BCO, (b) BCT10, (c) BCT20, (d) BCT30, and (e) BCT40.

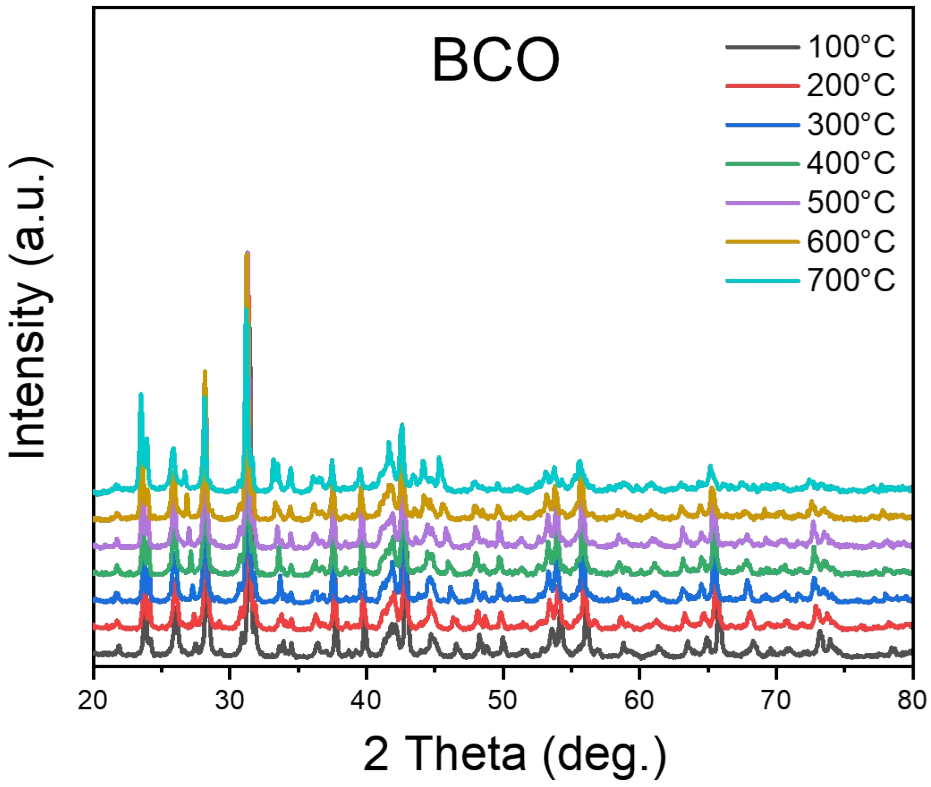

Figure S9. High-temperature X-ray diffraction (XRD) profiles of $BaCoO_{3-\delta}$ (BCO)

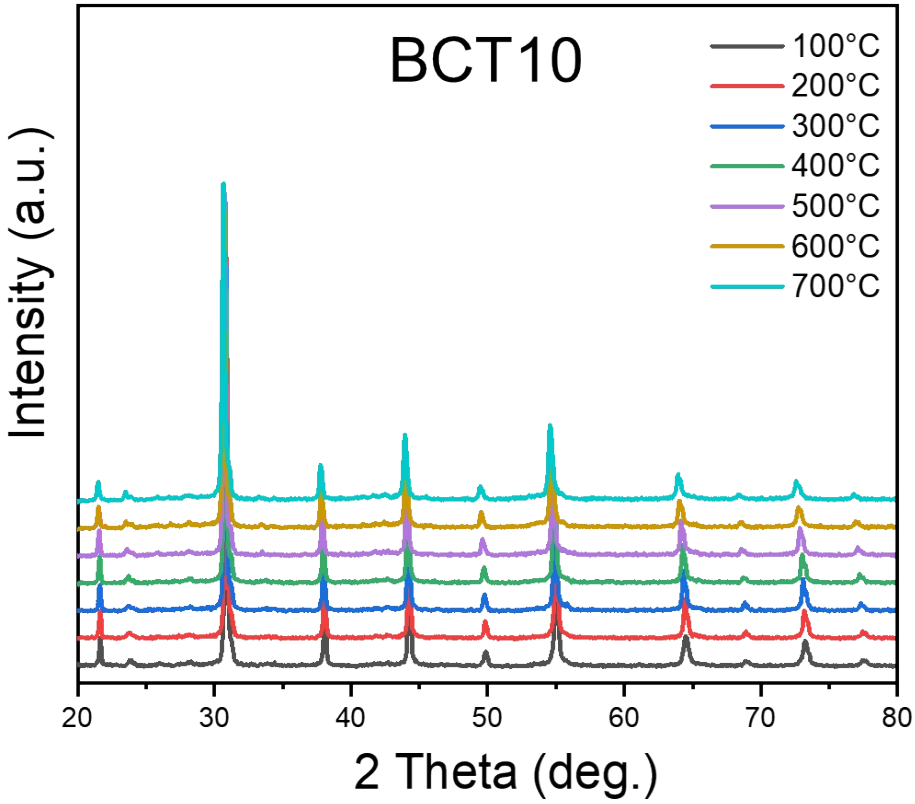

Figure S10. High-temperature X-ray diffraction (XRD) profiles of $BaCo_{0.9}Ta_{0.1}O_{3-\delta}$ (BCT10)

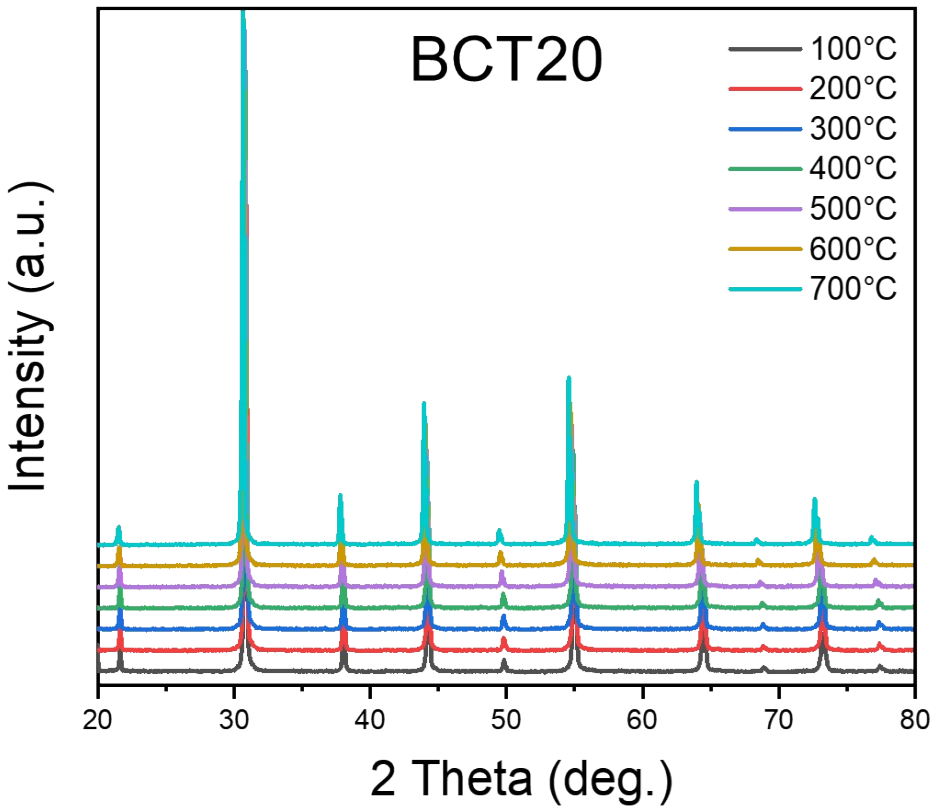

Figure S11. High-temperature X-ray diffraction (XRD) profiles of $BaCo_{0.8}Ta_{0.2}O_{3-\delta}$ (BCT20)

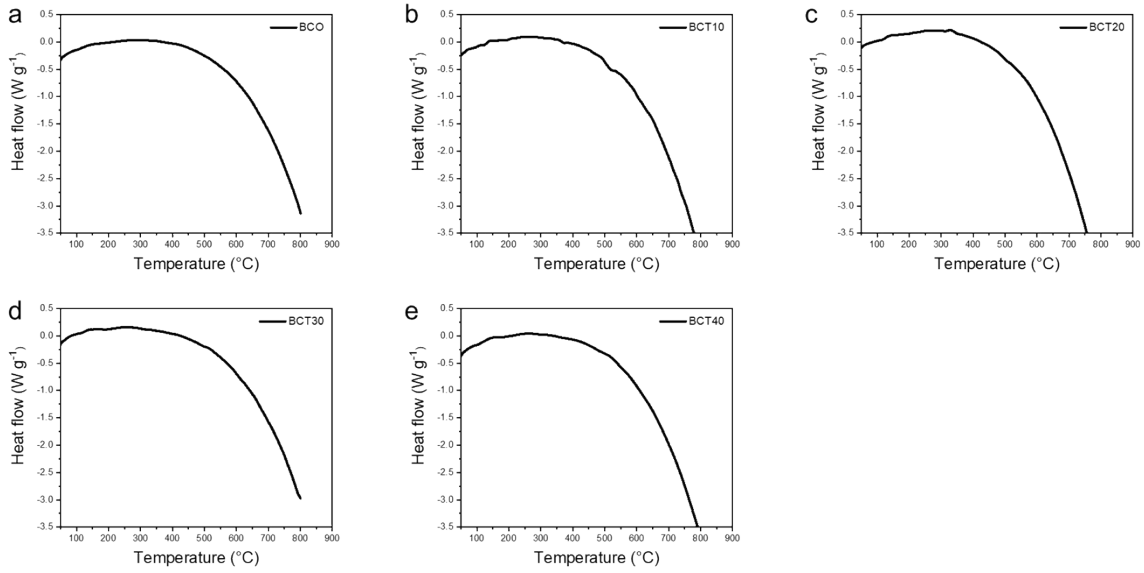

Figure S12. DSC profiles from room temperature to 800°C of (a) BCO, (b) BCT10, (c) BCT20, (d) BCT30, and (e) BCT40.

Supplementary note:

Generally, heating up of an oxide can result in several structural changes, and its outcome can vary from materials to materials; Some oxides may experience lattice parameter expansion or others can experience thermally induced phase transition.

For example, recent studies show that hexagonal perovskites and their derivatives form an important new family of materials with high ionic conductivity,[4-6] and it was reported that structural transitions of hexagonal perovskites are often observed during temperature increase. For example, Matthew et al., reported that $Ba_3NbMoO_{8.5}$ shows first-order phase transition around ~150 and ~350°C, which associated with the redistribution of metal atoms during heating.[4] Accordingly, it creates largely unoccupied oxygen sites which provides high oxide ion conductivity for hexagonal perovskites. Similar results have been suggested by Fop et al., with $Ba_7Nb_4MoO_{20}$, that oxygen fractional occupancies at palmierite-like layers are reorganized above 290°C, and these partially occupied oxygen sites provide high oxygen ion and proton conductivity.[5]

As the structural transition found in hexagonal perovskites are intimately associated with superior ionic conductivity, it is thus very important to investigate whether such a structure transition can occur on BCT10. We expected that similar thermal transition will occur on

BCT10 as seen in those of hexagonal perovskites, however our high temperature XRD result implied that BCT10 seemed to have no phase transition. The DSC of BCT10 displayed no assignable thermal phase-transition peak as well. Instead, BCT10 showed lattice parameter expansion which we ascribe to the thermal loss of oxygen from the bulk crystal.

There may be several reasons to explain above phenomenon. First of all, the nanoscale domain of cubic-hexagonal interface resides in BCT10 may makes it difficult to characterize the structural changes with XRD. As described in the Figure S3, streaking SAED patterns of BCT10 suggests stacking faults exists between BCT10's cubic-hexagonal phases, which is hardly detected with the resolution of XRD characterization.

Secondly, the different metal cation stoichiometry of BCT10 (i.e., A : B = 1 : 1), contrast to $Ba_3NbMoO_{8.5}$ (A : B = 1.5 : 1) or $Ba_7Nb_4MoO_{20}$ (A : B = 1.4 : 1) may prevent thermally induced phase transition behavior. Hence, to implement high-temperature structure transition for hexagonal BCT system, a stoichiometric compound of Ba_3CoTaO_x or $Ba_7Co_4TaO_x$ can be investigated in the future for their use of next-generation SOFC air-electrodes.

Lastly, the temperature we investigated (i.e., room temperature to 700^{o}C) may provide too narrow temperature window to induce thermal-phase transition for BCT10. In other words, a higher temperature >800^{o}C may be needed to realize thermal-phase transition for BCT10.

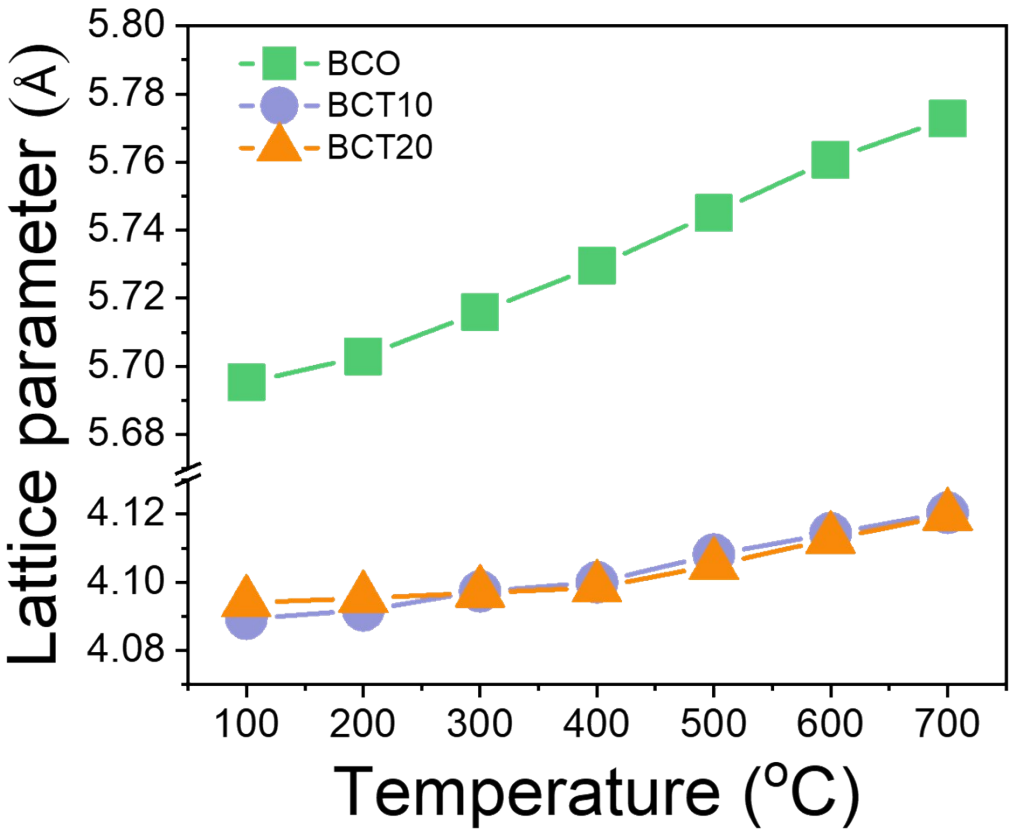

Figure S13. Lattice parameter expansion of the $BaCoO_{3-\delta}$ (BCO), $BaCo_{0.9}Ta_{0.1}O_{3-\delta}$ (BCT10), and $BaCo_{0.8}Ta_{0.2}O_{3-\delta}$ (BCT20) as a function of the temperature

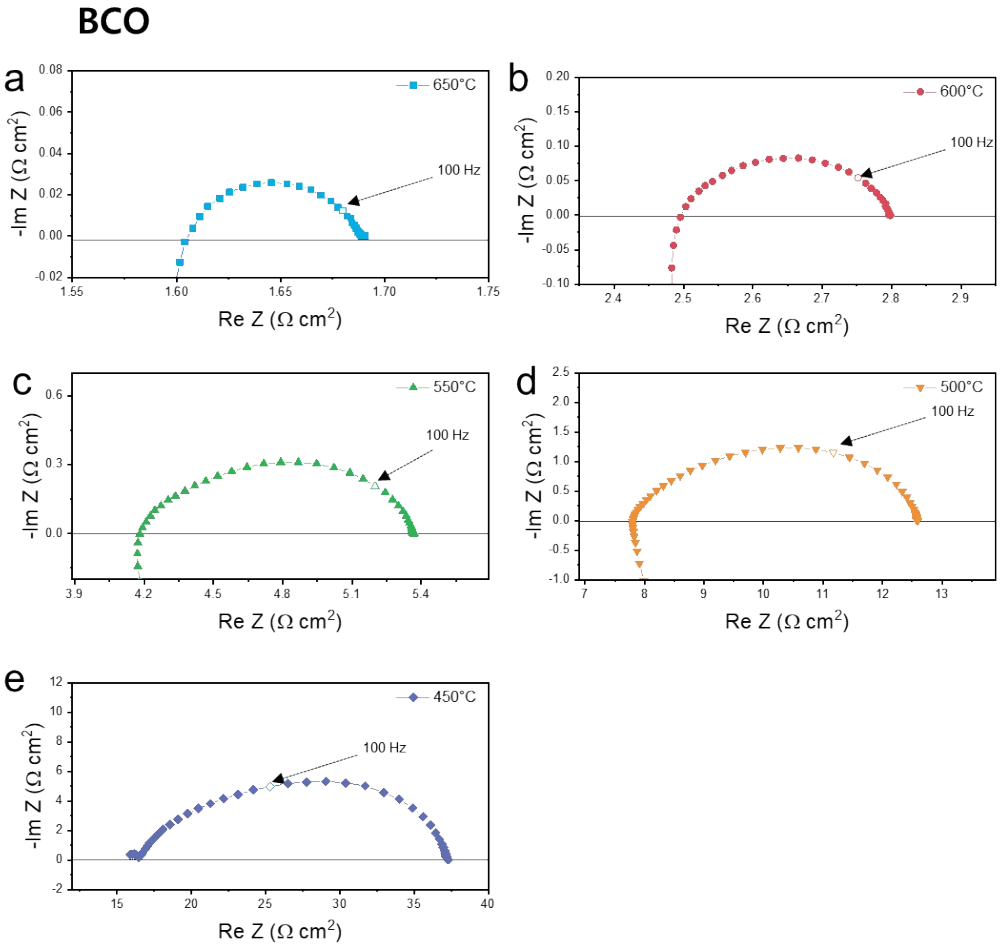

Figure S14. Impedance data sets for porous BCO electrode using SDC symmetric cell configuration. (a) 650°C, (b) 600°C, (c) 550°C, (d) 500°C, (e) 450°C.

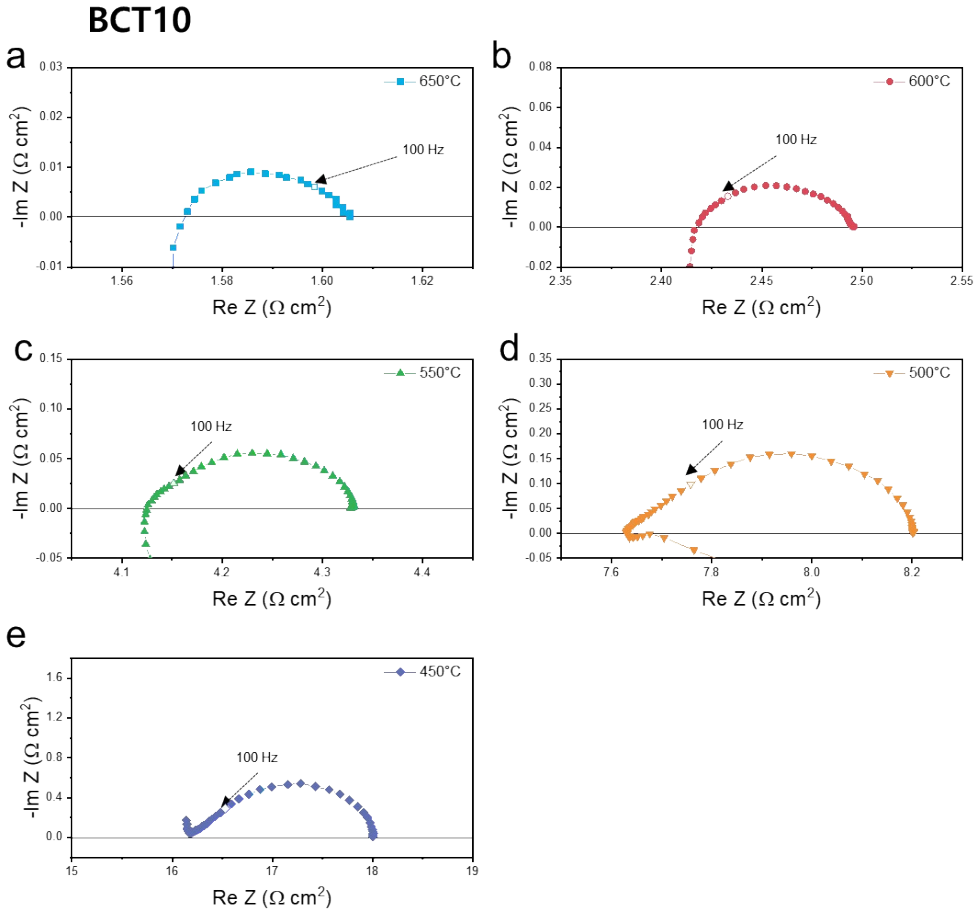

Figure S15. Impedance data sets for porous BCT10 electrode using SDC symmetric cell configuration. (a) 650°C, (b) 600°C, (c) 550°C, (d) 500°C, (e) 450°C.

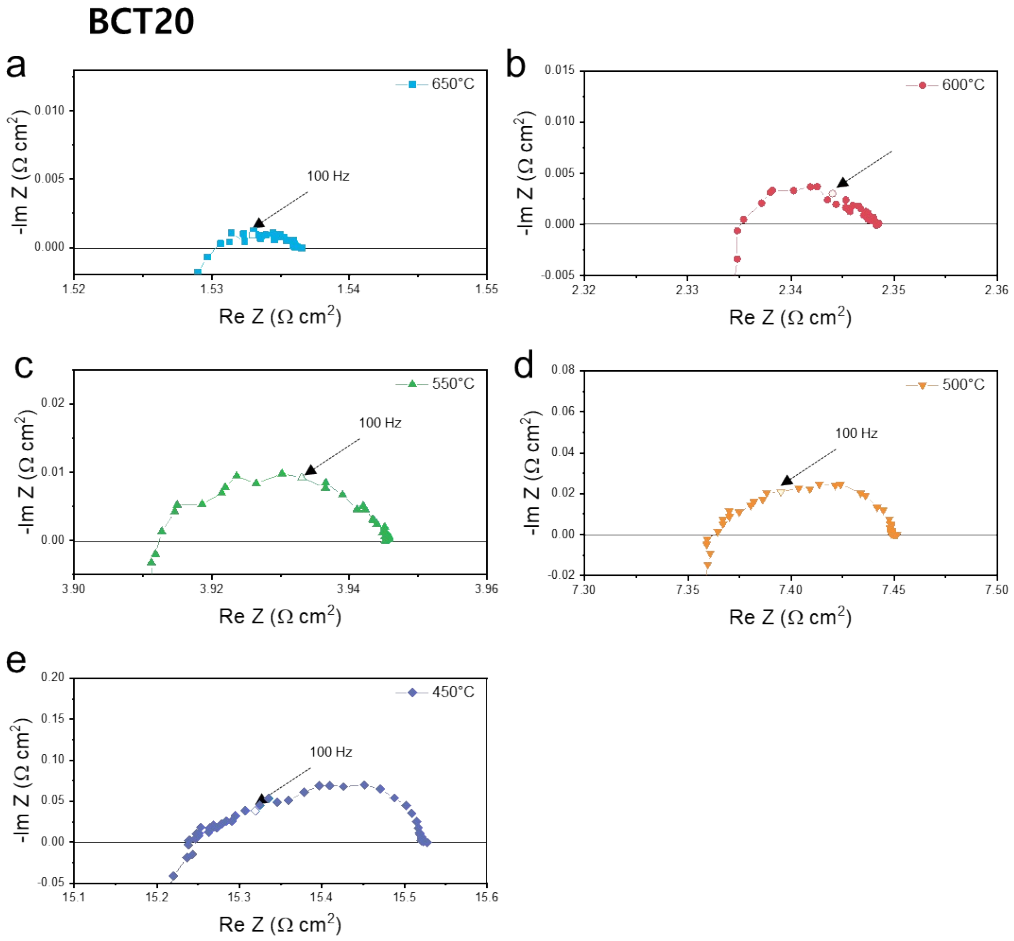

Figure S16. Impedance data sets for porous BCT10 electrode using SDC symmetric cell configuration. (a) 650°C, (b) 600°C, (c) 550°C, (d) 500°C, (e) 450°C.

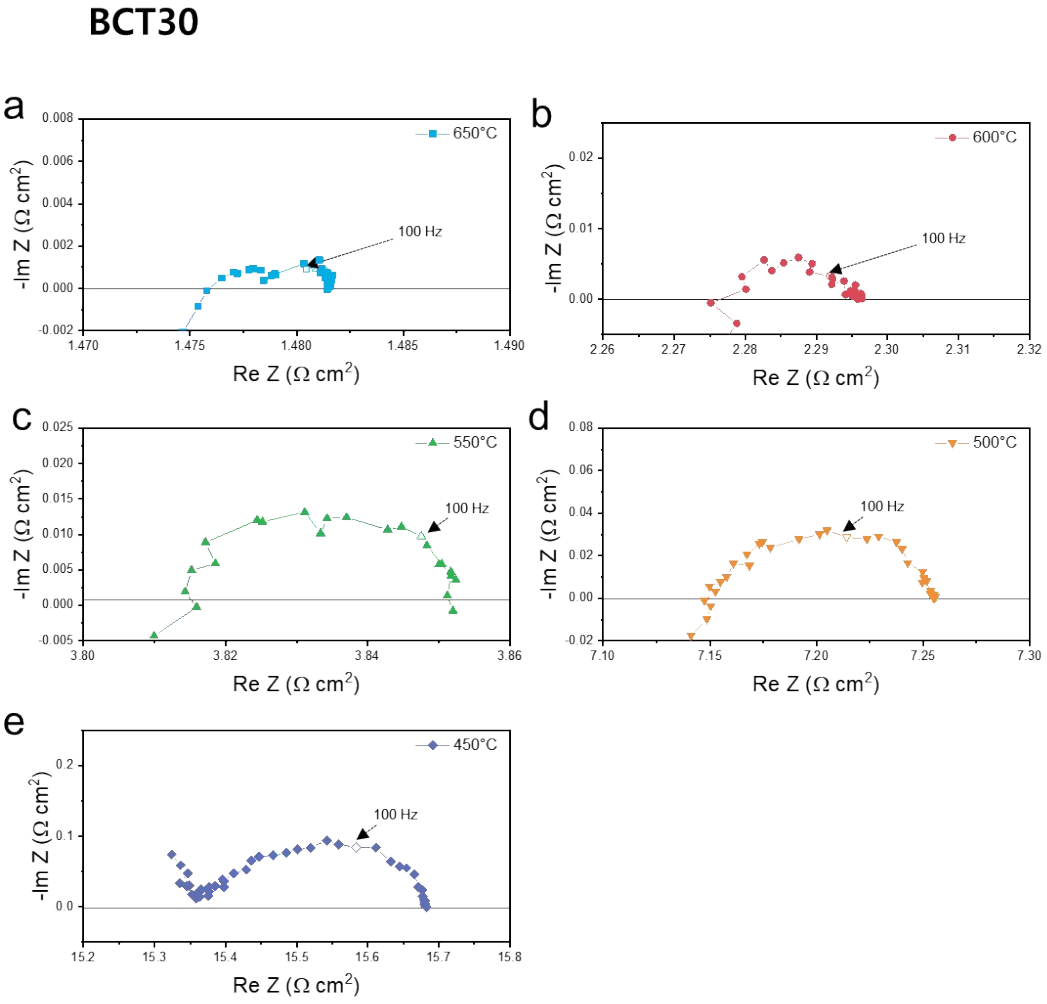

Figure S17. Impedance data sets for porous BCT30 electrode using SDC symmetric cell configuration. (a) 650°C, (b) 600°C, (c) 550°C, (d) 500°C, (e) 450°C.

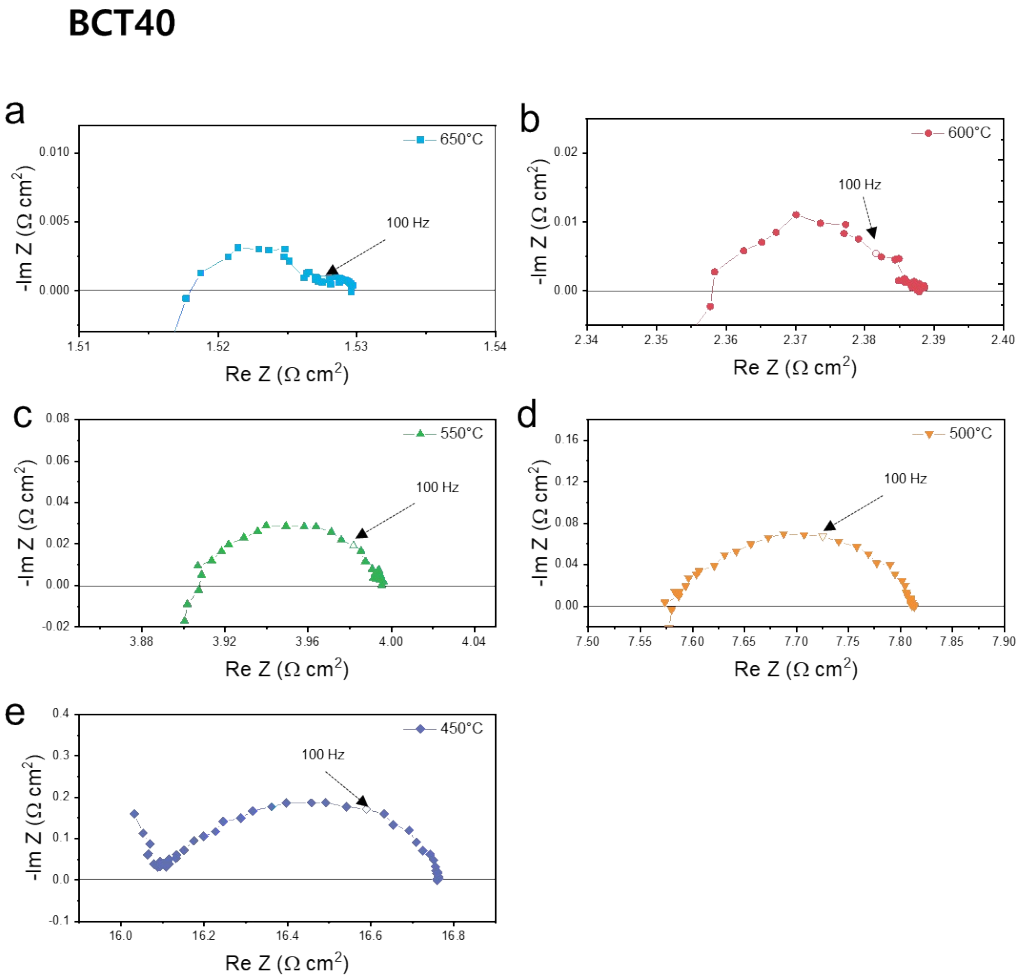

Figure S18. Impedance data sets for porous BCT40 electrode using SDC symmetric cell configuration. (a) 650ºC, (b) 600ºC, (c) 550ºC, (d) 500ºC, (e) 450ºC.

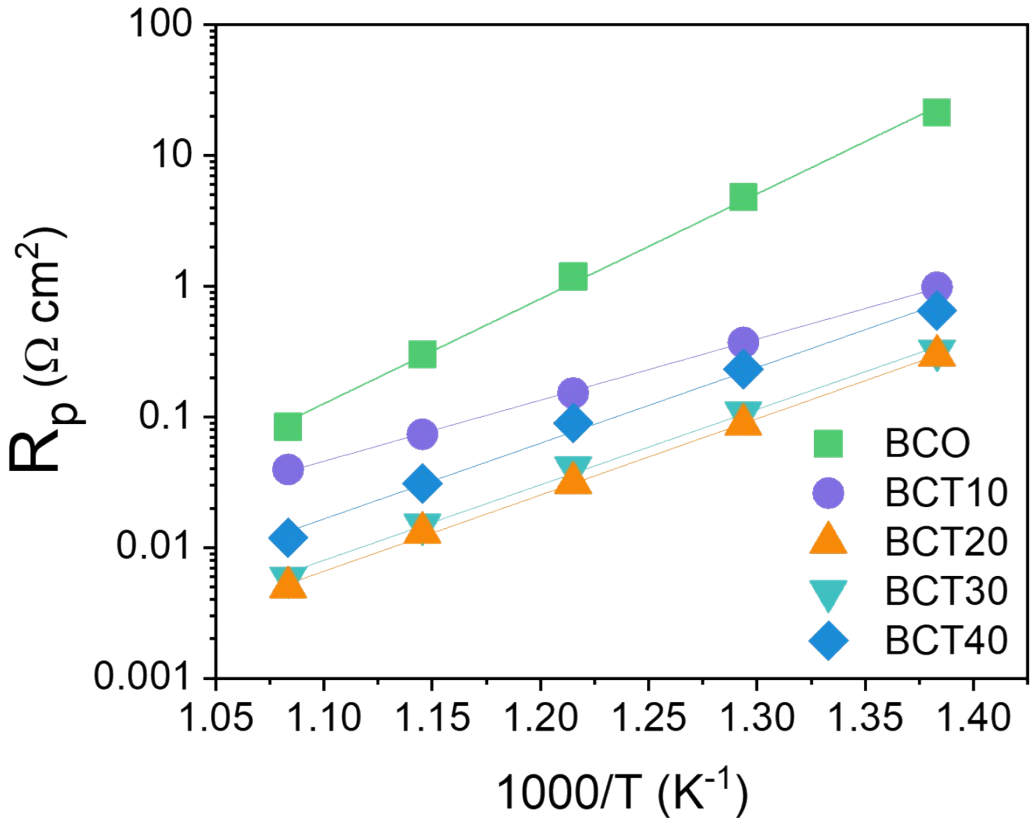

Figure S19. Arrhenius plots of polarization resistance (R_p) for $BaCo_{1-x}Ta_xO_{3-\delta}$ (X = 0, 0.1, 0.2, 0.3 and 0.4, which are noted as BCO, BCT10, BCT20, BCT30 and BCT40, respectively). Data sets of BCT10 was from previous study.[7]

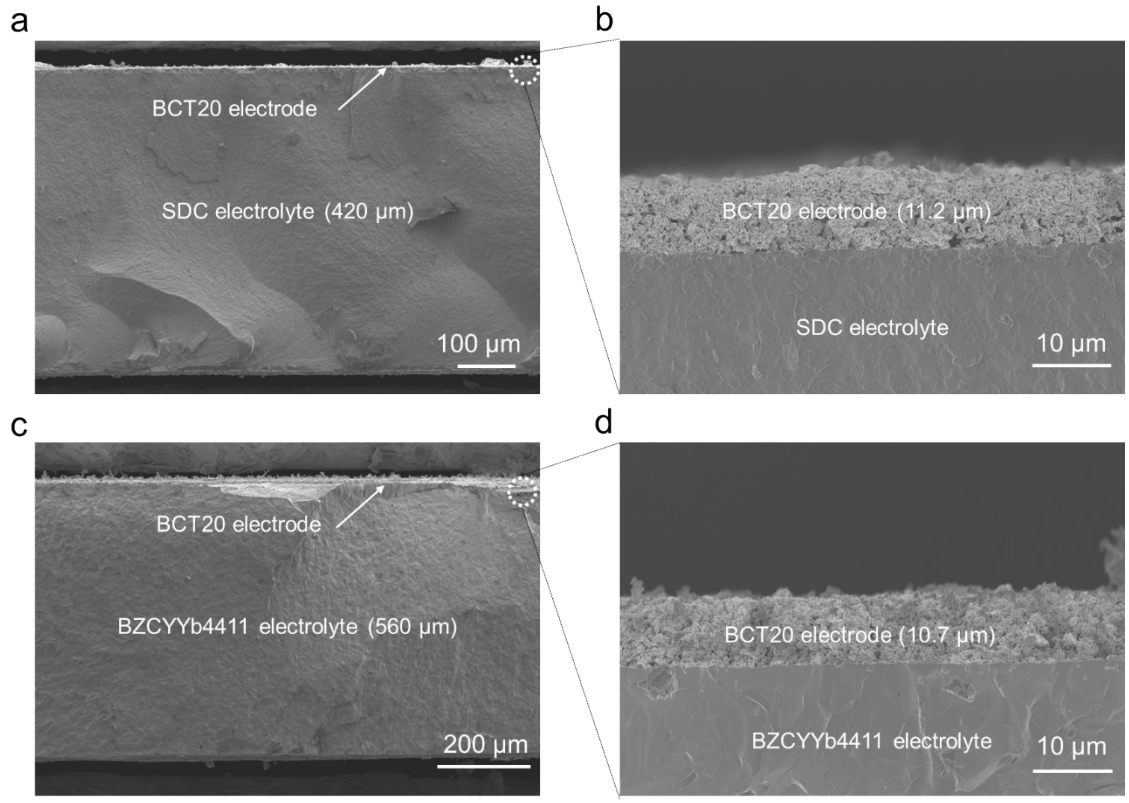

Figure S20. (a) Cross sectional SEM image of the symmetric cell based on SDC electrolyte (b). Scanning electron microscope (SEM) image focused on oxygen-electrode on SDC electrolyte. (c) Cross sectional SEM image of the symmetric cell based on BZCYYb4411 electrolyte. (d) Scanning electron microscope (SEM) image focused on oxygen-electrode on BZCYYb4411 electrolyte.

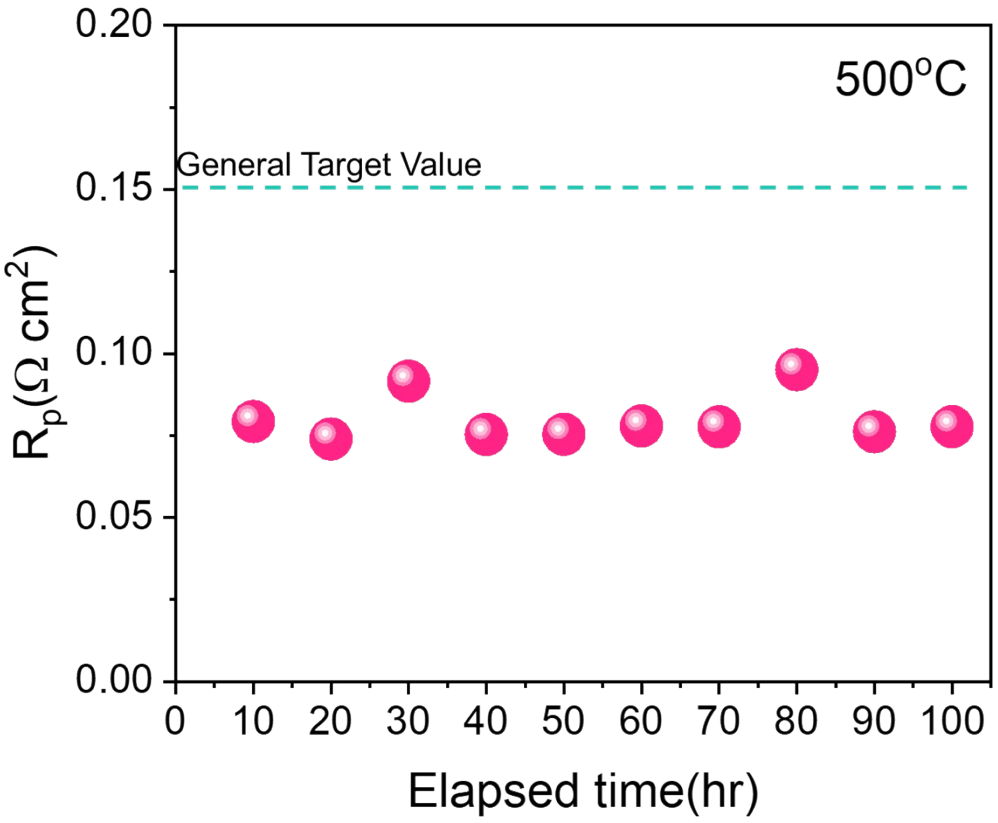

Figure S21. Short-term stability tests of BCT20|SDC|BCT20 symmetric cell in synthetic air (pO_2 = 0.21 atm)

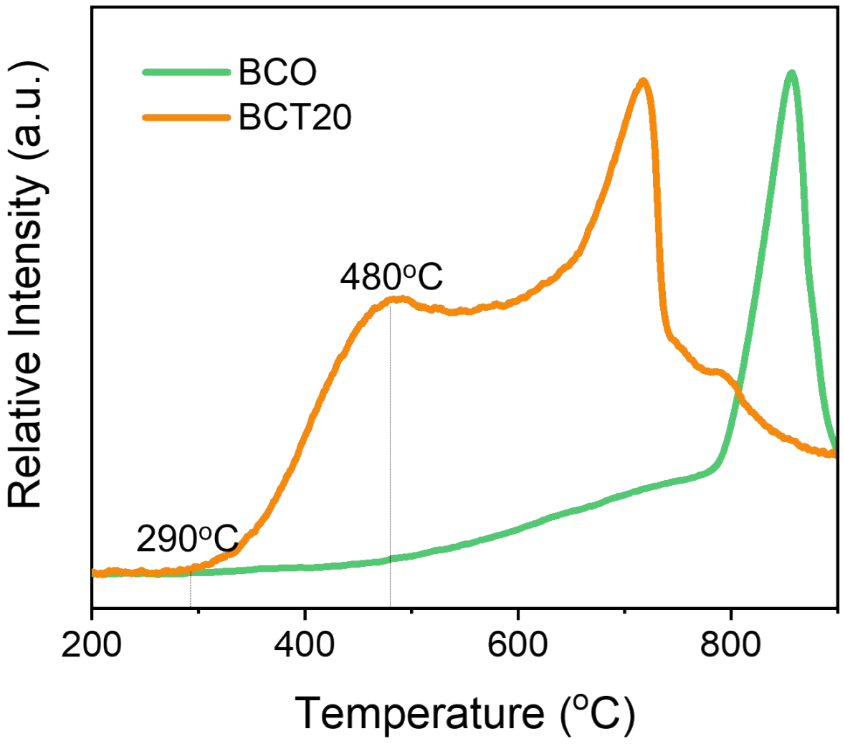

Figure S22. O_2-TPD profiles of BCT20 and BCO samples

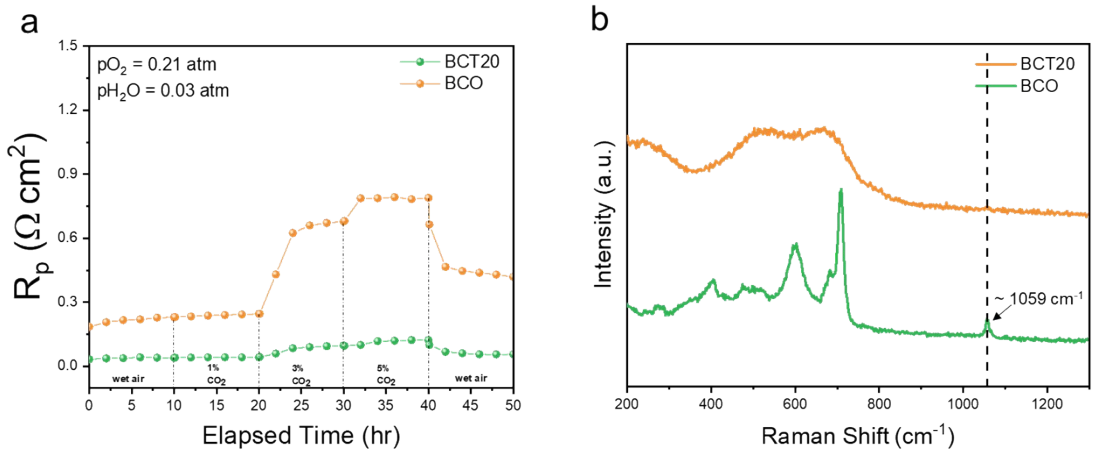

Figure S23. (a) EIS profiles of BCT20 and pure BCO at different CO_2 concentrations. (b) Raman spectra after 18 hours heat treatment at 600°C, in a 2 vol.% CO_2 atmosphere.

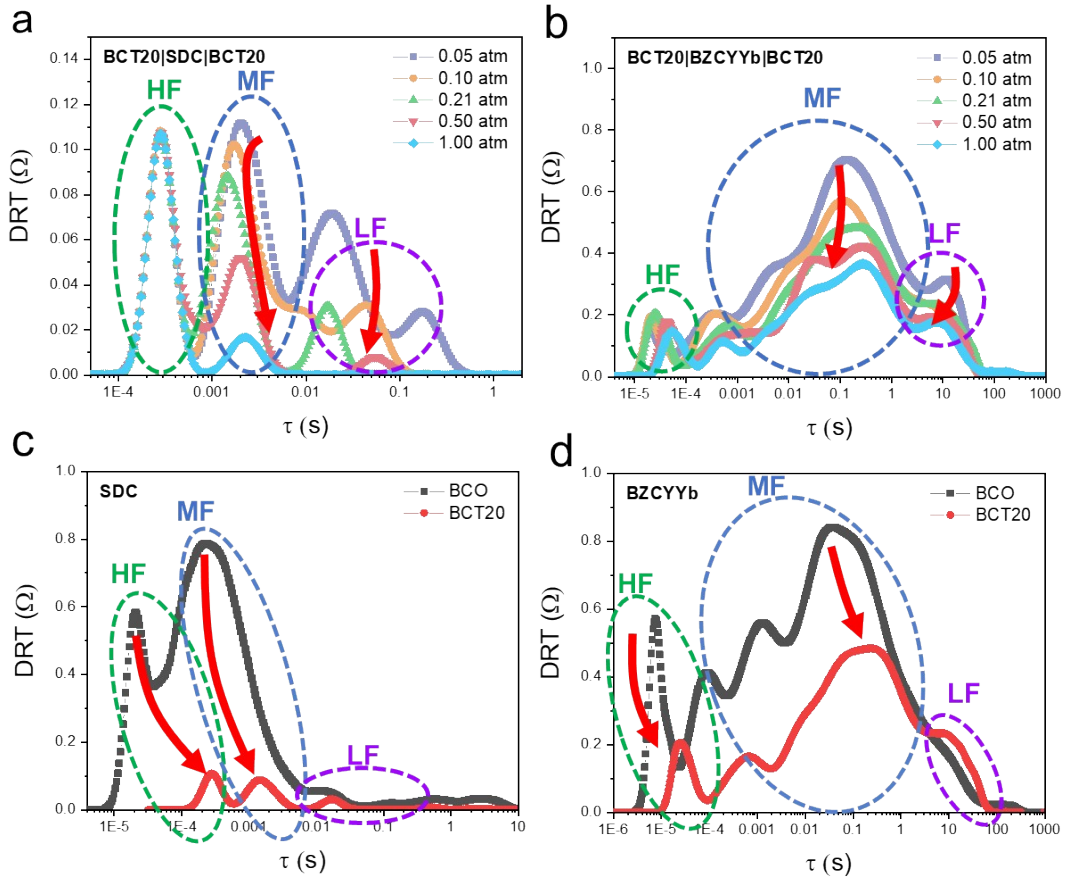

Figure S24. Impacts of oxygen partial pressure on the distribution of relaxation time (DRT) functions of porous BCT20 electrodes on (a) SDC electrolyte and (b) BZCYYb electrolyte at 550°C. Comparison of DRT functions between BCT20 and BCO on (c) SDC electrolyte and (d) BZCYYb electrolyte at 0.21 atm, 550°C.

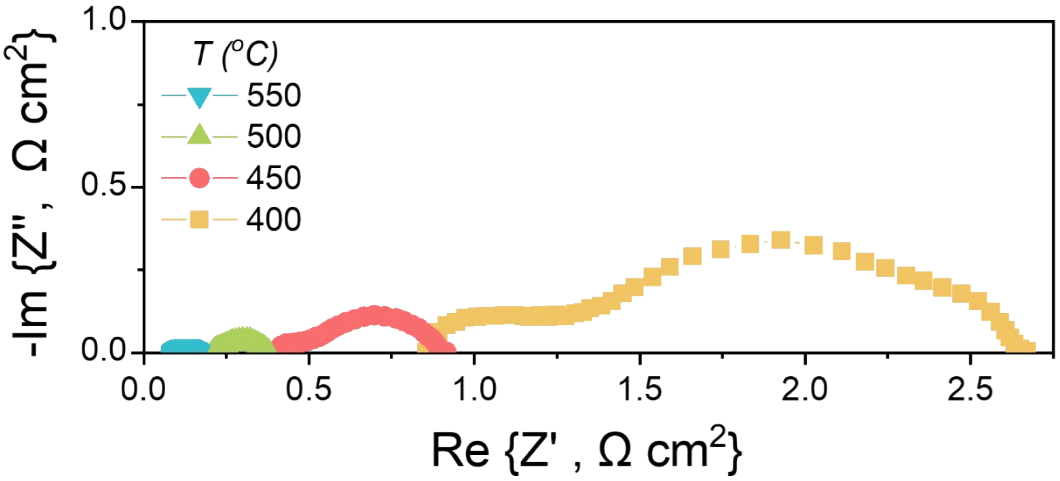

Figure S25. Electrochemical impedance spectroscopy (EIS) of the GDC-based single cell

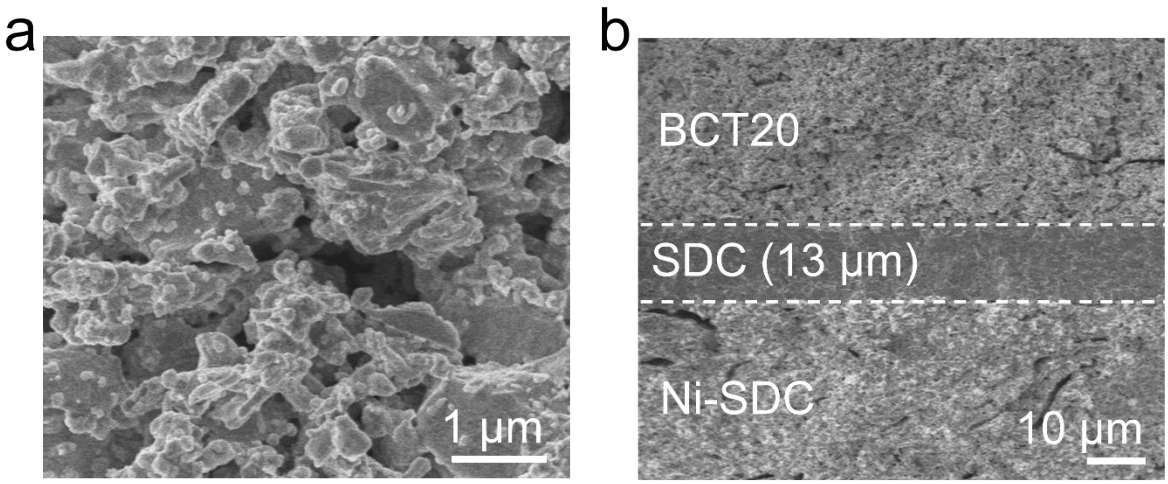

Figure S26. Scanning electron microscope (SEM) image depicting porous cathode microstructures of BCT20. (e) Cross-sectional SEM image of the SDC based-single cell.

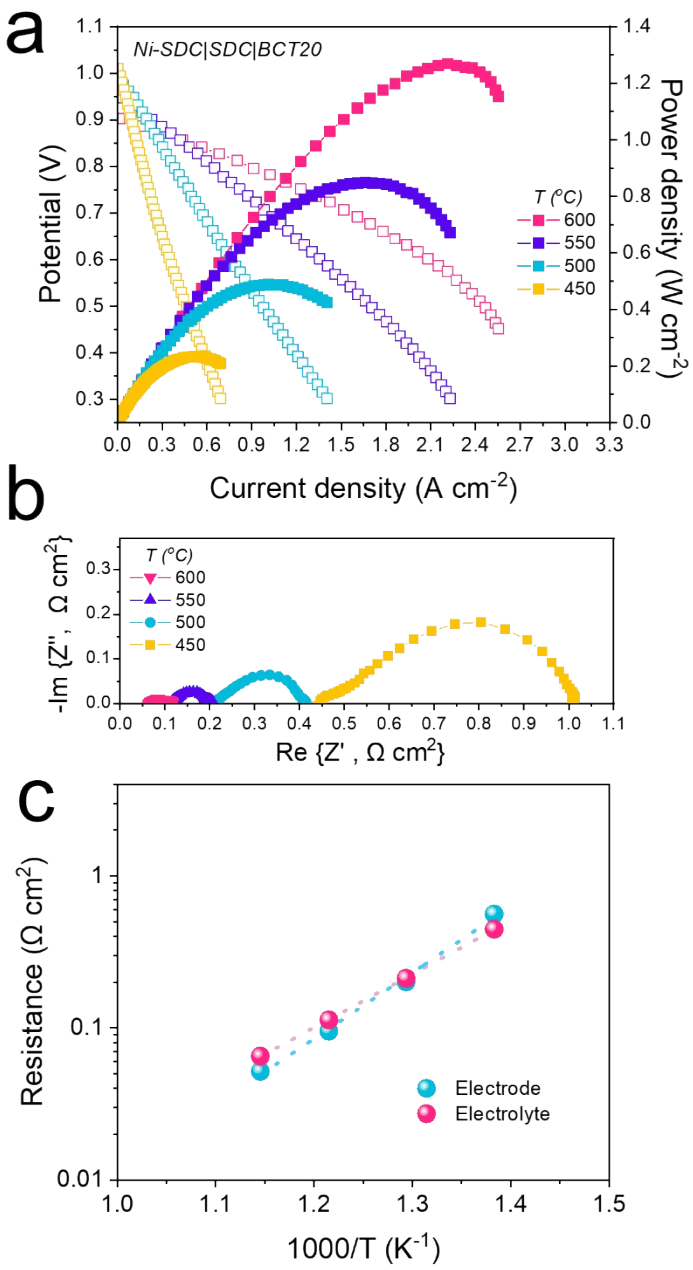

Figure S27. (a) Typical I-V-P curves of a single cell with a configuration of Ni-$Sm_{0.2}Ce_{0.8}O_{2-\delta}$ (SDC)|SDC|$BaCo_{0.8}Ta_{0.2}O_{3-\delta}$ (BCT20) at temperature range of 450~600°C. (b) electrochemical impedance spectroscopy (EIS) of the SDC-based single cell and according (c) Arrhenius plots of electrode and electrolyte resistances.

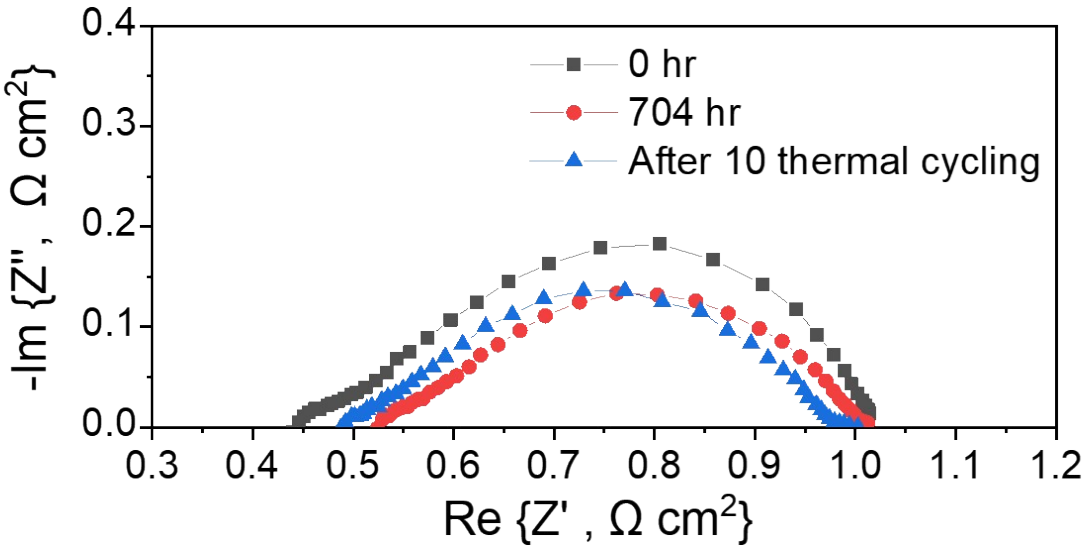

Figure S28. Comparison of impedance spectra of SDC-based single cell measured before and after 704 hours of long-term operation and additional 10 rapid thermal cycling.

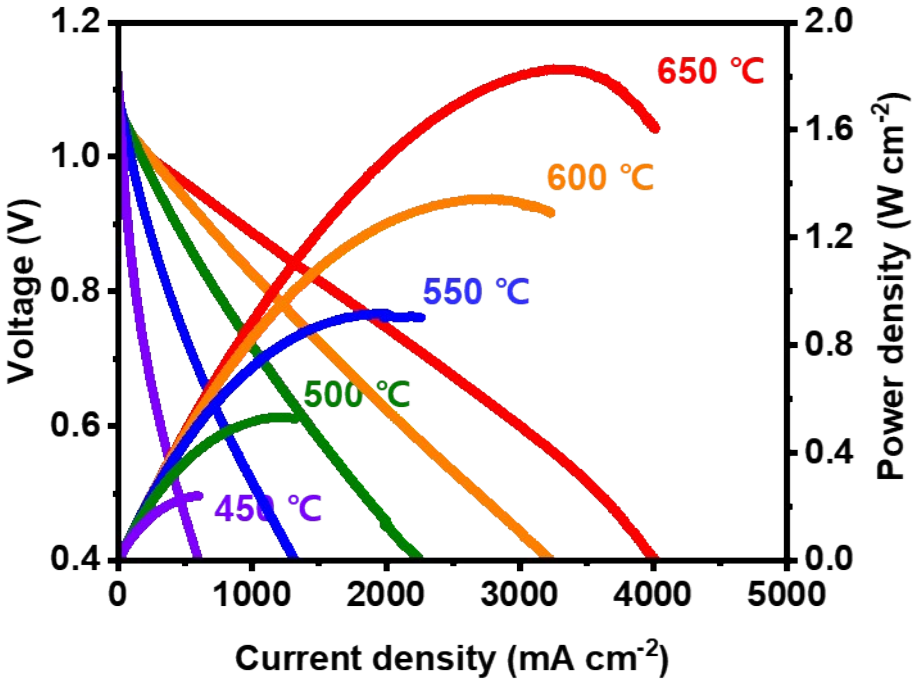

Figure S29. Typical I-V-P curves of a single cell with a configuration of Ni-$BaZr_{0.4}Ce_{0.4}Y_{0.1}Yb_{0.1}O_{3-\delta}$ (BZCYYb)|BZCYYb|BCT20, without additional PLD layer at temperature range of 450~650°C.

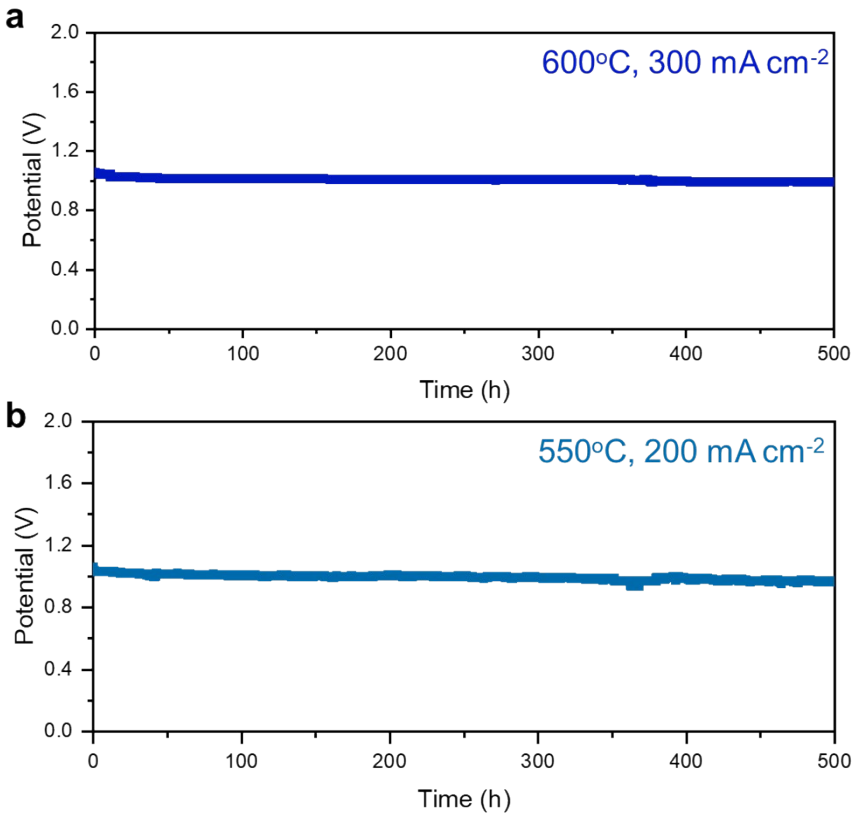

Figure S30. Long-term durability tests of the PCFC single cell with BCT20 oxygen-electrode. (a) at 600°C with an applied current of 300 mA cm^{-2} and (b) at 550°C with an applied current of 200 mA cm^{-2}.

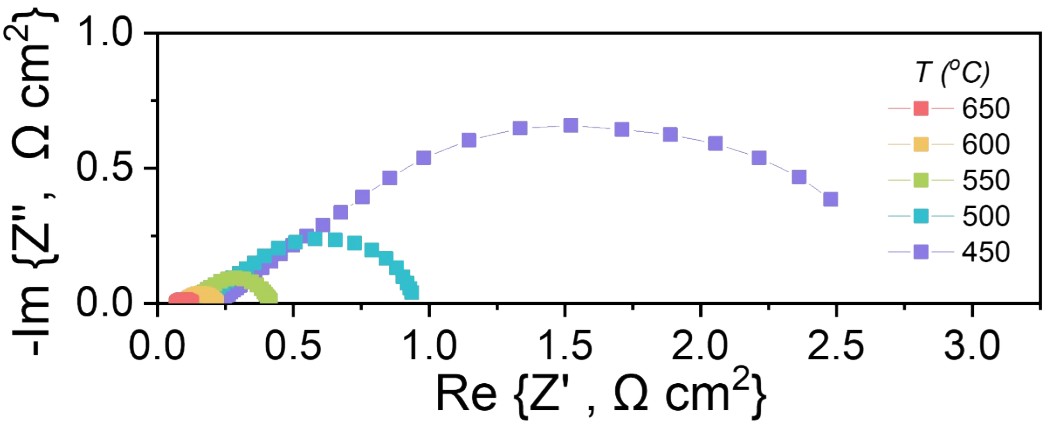

Figure S31. Electrochemical impedance spectroscopy (EIS) of the single cell with the geometry of Ni-$BaZr_{0.4}Ce_{0.4}Y_{0.1}Yb_{0.1}O_{3-\delta}$ (BZCYYb)|BZCYYb|BCT20, with additional PLD layer.

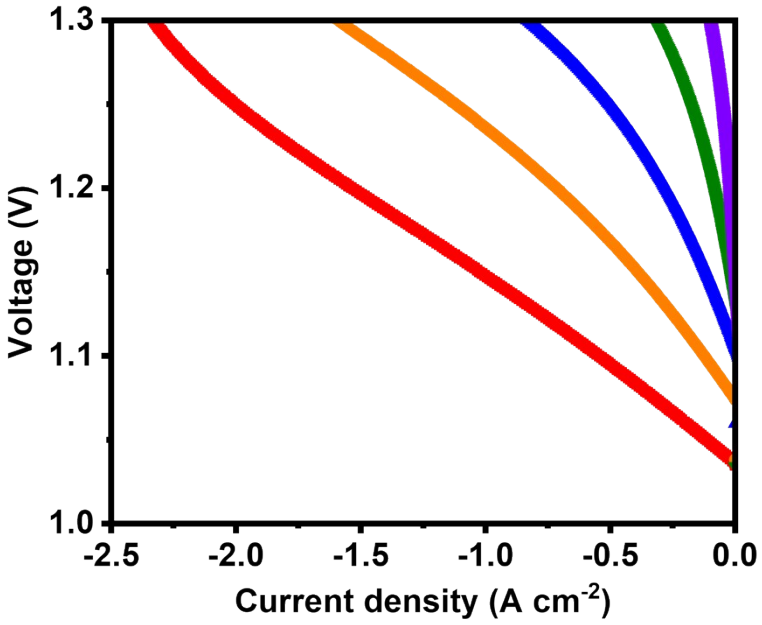

Figure S32. Typical I-V curves of a single cell with a configuration of Ni-$BaZr_{0.4}Ce_{0.4}Y_{0.1}Yb_{0.1}O_{3-\delta}$ (BZCYYb)|BZCYYb|BCT20, with additional PLD layer at temperature range of 450~650^{o}C.

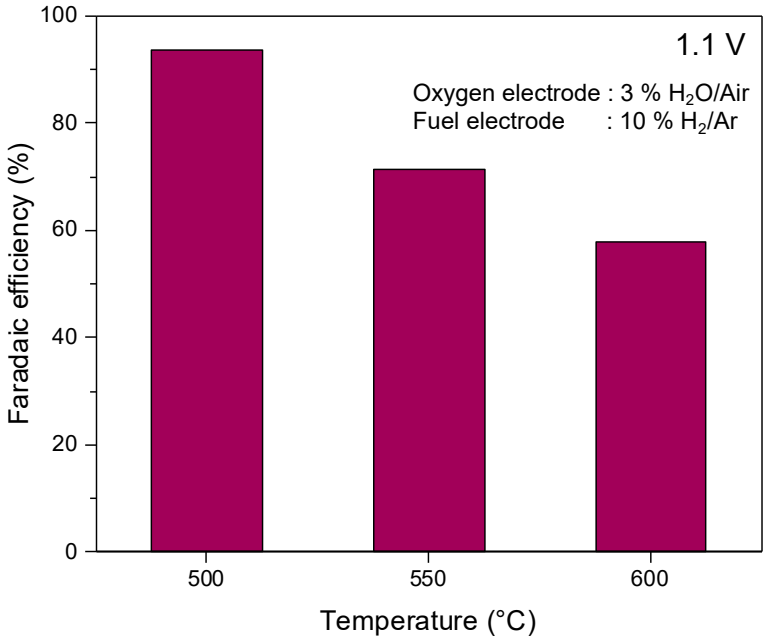

Figure S33. Faradaic efficiencies of the proton-conducting SOCs with a configuration of Ni-BZCYYb|BZCYYb|BCT20 in temperature range of 500~600 °C at 1.1 V. Humidified (3 % H_2O) air was fed to the oxygen-electrode and 10% H_2/Ar gas was exposed to the fuel-electrode. The BCT20 electrolysis cell achieved Faradaic efficiencies comparable to values from recently reported protonic ceramic electrolysis cells.[8, 9]

References

1. H. Yu, H. N. Im and K. T. Lee, *Advanced Functional Materials*, 2022, **32**, 2207725.
2. D. Kim, K. T. Bae, K. J. Kim, H.-N. Im, S. Jang, S. Oh, S. W. Lee, T. H. Shin and K. T. Lee, *ACS Energy Letters*, 2022, **7**, 2393-2400.
3. T. G. Yun, Y. Heo, H. Bin Bae and S.-Y. Chung, *Nature Communications*, 2021, **12**, 824.
4. M. S. Chambers, K. S. McCombie, J. E. Auckett, A. C. McLaughlin, J. T. Irvine, P. A. Chater, J. S. Evans and I. R. J. J. o. M. C. A. Evans, *Journal of Materials Chemistry A*, 2019, **7**, 25503-25510.
5. S. Fop, K. S. McCombie, E. J. Wildman, J. M. Skakle, J. T. Irvine, P. A. Connor, C. Savaniu, C. Ritter and A. C. Mclaughlin, *Nature materials*, 2020, **19**, 752-757.
6. M. Yashima, T. Tsujiguchi, Y. Sakuda, Y. Yasui, Y. Zhou, K. Fujii, S. Torii, T. Kamiyama and S. J. Skinner, *Nature communications*, 2021, **12**, 556.
7. J. H. Kim, J. K. Kim, H. G. Seo, D. K. Lim, S. J. Jeong, J. Seo, J. Kim and W. Jung, *Adv. Funct. Mater.*, 2020, 2001326.
8. S. Choi, T. C. Davenport and S. M. Haile, *Energy & Environmental Science*, 2019, **12**, 206-215.
9. C. Duan, R. Kee, H. Zhu, N. Sullivan, L. Zhu, L. Bian, D. Jennings and R. O'Hayre, *Nature Energy*, 2019, **4**, 230.